physica status solidi rrl
www.pss-rapid.com

Check for updates

From Doping to Dilution: Local Chemistry and Collective Interactions of La in HfO_2

Thomas Szyjka, Lutz Baumgarten, Oliver Rehm, Claudia Richter, Yury Matveyev, Christoph Schlueter, Thomas Mikolajick, Uwe Schroeder, and Martina Müller*

Lanthanum (La) doping is considered as a promising route to overcome reliability issues of switchable ferroelectric HfO_2-based devices. This study links the local chemistry at the La lattice sites with local and collective electronic properties of the La:HfO_2 matrix using hard X-ray photoelectron spectroscopy. The satellite structure of the La 3*d* core level, the plasmonic excitation energies, and core-level rigid binding energy shifts are investigated for La:HfO_2 samples with a wide range of La doping, ranging from 3.5% to 33%, i.e., from the doping to dilution level. The emerging chemical phases and electronic properties are discussed as a function of La content. From the evolution of the plasmon excitation energies and rigid binding energy shifts, it is concluded that electronic charge compensation by oxygen vacancies occurs for increasing La content.

1. Introduction

HfO_2-based thin films bear huge potential for the next generation of nonvolatile memory applications. They provide the functional part of numerous device concepts like, e.g., resistive random access memory (RRAM), switchable ferroelectrics (FE) of metal–FE–metal capacitor stacks in FE random access memory (FeRAM),[1] or metal–FE–semiconductor stacks in FE field-effect transistors (FeFET).[2,3] However, the application of HfO_2-based thin films as active ferroelectrics in FeRAM or FeFET devices is still impaired by reliability issues like wake-up, imprint, and fatigue, which compromise a durable FE switching behavior.

Since the unexpected formation of a ferroelectric phase of HfO_2 was observed by Boescke et al.,[4] HfO_2-based compounds are under intense investigation. The structural stabilization of FE HfO_2 is mainly realized by controlled lattice strain, which, for example, can be achieved by introducing a certain amount of intrinsic defects like oxygen vacancies (OVs).[5] The role of OV is, however, twofold: on the one hand, OVs stabilize the FE phase, but on the other hand, they weaken the ferroelectric behavior by causing FE domain pinning or charge trapping causing leakage currents. Another route to create controlled lattice strain is by stabilizing the ferroelectric HfO_2 phase by extrinsic ion doping.[3,6,7] Both anion and cation doping is currently explored to stabilize the ferroelectric phase of HfO_2 and to improve the switchability of FE devices.[8,9] The latter effect may be achieved either by a reduction of the OV density itself or by an electronic compensation of the vacancy charges and states.

A variety of cation dopants were investigated experimentally and theoretically, i.e., Si, Al, Sr, La, Gd, Y, and Sc.[7] Among those, lanthanum turned out to be the most promising candidate for a CMOS compatible stabilization of the FE phase of HfO_2 with large FE polarization. In particular, La doping permits for applying rather low annealing temperatures (400 °C) required for recrystallization, which are essential for CMOS device processing. In this way, large and homogeneous doping concentrations are realized for La at rather low preparation temperatures in contrast to other dopants.

Due to its larger ionic radius compared to Hf, La distorts the HfO_2 lattice and can stabilize the ferroelectric phase. Theoretically, lanthanum is predicted to structurally stabilize the ferroelectric phase for doping concentrations up to 6%.[10–13] Experimentally, FE properties were observed for a wide range of doping concentrations between 6% and 16%, with a maximum FE polarization at a La concentration of about 11%.[9] For La concentrations above 15%, the FE polarization decreases and vanishes at about 20%, which is related to the formation of the cubic phase.[9] Perevalov et al. concluded from a shape

T. Szyjka, O. Rehm, M. Müller
Fachbereich Physik
Universität Konstanz
78457 Konstanz, Germany

T. Szyjka, L. Baumgarten
Forschungszentrum Jülich GmbH
Peter Grünberg Institut (PGI-6)
52425 Jülich, Germany
E-mail: l.baumgarten@fz-juelich.de

C. Richter, T. Mikolajick, U. Schroeder
NaMLab gGmbH
Noethnitzer Str. 64a, 01187 Dresden, Germany

Y. Matveyev, C. Schlueter
Deutsches Elektronen-Synchrotron
Notkestraße 85, 22607 Hamburg, Germany

T. Mikolajick
Chair of Nanoelectronic
TU Dresden
01062 Dresden, Germany

The ORCID identification number(s) for the author(s) of this article can be found under https://doi.org/10.1002/pssr.202100582.

© 2022 The Authors. physica status solidi (RRL) Rapid Research Letters published by Wiley-VCH GmbH. This is an open access article under the terms of the Creative Commons Attribution-NonCommercial-NoDerivs License, which permits use and distribution in any medium, provided the original work is properly cited, the use is non-commercial and no modifications or adaptations are made.

DOI: 10.1002/pssr.202100582

© 2022 The Authors. physica status solidi (RRL) Rapid Research Letters published by Wiley-VCH GmbH

18626270, 2022, 10, Downloaded from https://onlinelibrary.wiley.com/doi/10.1002/pssr.202100582 by Forschungszentrum Jülich GmbH Research Center, Wiley Online Library on [05/12/2022]. See the Terms and Conditions (https://onlinelibrary.wiley.com/terms-and-conditions) on Wiley Online Library for rules of use; OA articles are governed by the applicable Creative Commons License

analysis of X-ray photoelectron spectroscopy (XPS) spectra on the formation of a La_2O_3 phase, which shall intermix with HfO_2 at a La content of 10%.[14] Structural investigations by Smirnova et al. revealed a pyrochlore $La_2Hf_2O_7$ phase formation above 18% La content,[15] which is in agreement with observations by Schroeder et al.[9] The XPS spectra of $La_2Hf_2O_7$ showed a similar shape of the La 3*d* core level as La_2O_3.

Direct insights into the chemical and electronic properties of solids are gained by photoelectron spectroscopy (PES) techniques by recording core levels and valence states element selectively. Hard X-ray photoelectron spectroscopy (HAXPES) gives access to the properties of buried interfaces due to an enhanced information depth[16,17] and thus enables the characterization of real-world devices.[18,19] For semiconductors and insulators, the so-called rigid binding energy (BE) shifts of the core levels can be directly assigned to changes of the Fermi-level position within the bandgap. In particular, these rigid BE shifts can be related to charged states, which may be created by doping or defects, and hence yield a direct signature of otherwise "invisible" defects. Moreover, the core-level PES spectra of rare-earth compounds like La are often dominated by satellites, which arise from many-body interactions of the core hole with the strongly localized but partially filled 4*f* levels. These pronounced satellite structures reflect the local chemical and electronic surrounding at the La lattice sites.

Here, we report on a HAXPES experiment of La-doped HfO_2 thin films with very different La contents (3.5%, 5%, 9%, and 33%), which refer to particular La:Hf layer stacking ratios applied during the atomic layer deposition (ALD) process (see **Figure 1**). These particular La:Hf ratios lead to ferroelectric polarizations around the maximum value as observed by Schroeder et al.[9] The general sample layout is depicted in Figure 1 as well.

In order to conclude on the chemical state of La:HfO_2 samples as a function of La concentration, we correlate the La 3*d* core-level spectral features to reference compounds of La_2O_3 and $La_2Hf_2O_7$ phases as reported in the literature. From this HAXPES data, we finally conclude on a compensation of the La hole doping by vacancies.

2. Results and Discussion

Doping HfO_2 by La cations results in a rather complex modification of the electronic structure: As a group III dopant, La creates holes in the valence band, which shift the Fermi level toward the valence band maximum. At a certain hole doping level, this energy shift favors the creation of additional OVs, which compensate these holes by supplying electrons. In this case, no additional Fermi-level shift can be achieved anymore because all additional holes are compensated by electrons provided by OVs. This situation is well known as the doping limit in semiconductors. In the case of La doping, Materlik et al. found that such electronic hole compensation by OV favors the ferroelectric phase compared to the monoclinic one.[12] In addition, the tetragonal and cubic phases were also favored by this interaction, which obviously contradicts experimental X-ray diffraction results. As pointed out by Materlik et al., this does not necessarily exclude the importance of hole–OV interactions. Furthermore, according to Liu et al.,[20] an interaction of holes with intrinsic OV may passivate the influence of these defects on the performance instabilities of the FE devices. As the FE phase of HfO_2 is typically stabilized at La concentrations between 5% and 15%, even the lowest concentration of 3.5% La investigated in this study is far above a typical doping concentration of electronic devices. Thus, a doping limit by the creation of additional vacancies or the interaction with intrinsic ones has to be taken into account for discussing the electronic structure of La-doped HfO_2.[21] We note that the abovementioned pyrochlore $La_2Hf_2O_7$ phase formally can be treated as a 50% La doping, which is electronically completely compensated by an OV (one missing oxygen per formal unit).

On the spectroscopic side, the most prominent electronic structure appears in the La 3*d* core levels as satellite peaks. **Figure 2** shows the La 3*d* core-level spectra for all samples with different La content in HfO_2. We find a spin–orbit split $3d_{5/2}$ and $3d_{3/2}$ multiplet located at about 834 and 851 eV BE, respectively. Each component is accompanied by a pronounced satellite peak located at about 5 eV larger BE. These satellites are related to an interaction of partially filled 4*f* orbitals with the core hole in the PES final state. At first glance, such an interaction shall be excluded in La, which has an unfilled 4*f* shell. However, the additional potential U_{fc} of the PES core hole shifts the unoccupied 4*f* levels down and below the Fermi level into the valence band. The latter mainly consists of the neighboring oxygen ligand orbitals. This process enables an occupation of the unfilled $4f^0$ state by the oxygen ligands, creating an occupied $4f^1$ state. In the early experimental and theoretical works,[22–24] these features have been considered as a double peak structure, which consists of the bonding and antibonding superposition of f^0 and f^1 contribution in the PES final state.[24] Due to improved experimental

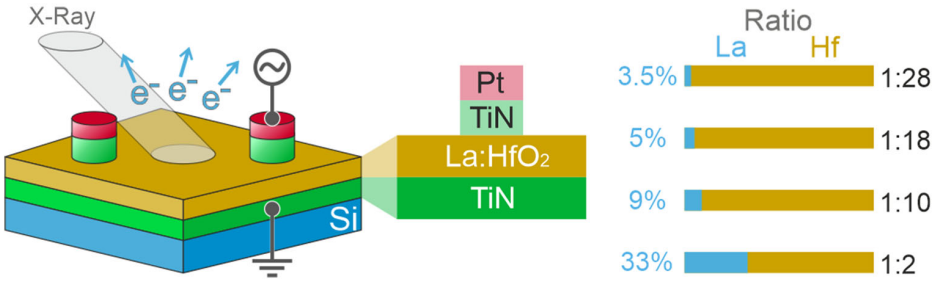

Figure 1. Schematics of the ferroelectric TiN/La:HfO_2/TiN sample stacks, investigated both by HAXPES and electric field cycling experiments. HAXPES was performed on areas between the top electrodes. The nominal La concentration is labeled according to the as-deposited La:Hf layer stacking ratio via ALD.

© 2022 The Authors. physica status solidi (RRL) Rapid Research Letters published by Wiley-VCH GmbH

18626270, 2022, 10, Downloaded from https://onlinelibrary.wiley.com/doi/10.1002/pssr.202100582 by Forschungszentrum Jülich GmbH Research Center, Wiley Online Library on [05/12/2022]. See the Terms and Conditions (https://onlinelibrary.wiley.com/terms-and-conditions) on Wiley Online Library for rules of use; OA articles are governed by the applicable Creative Commons License

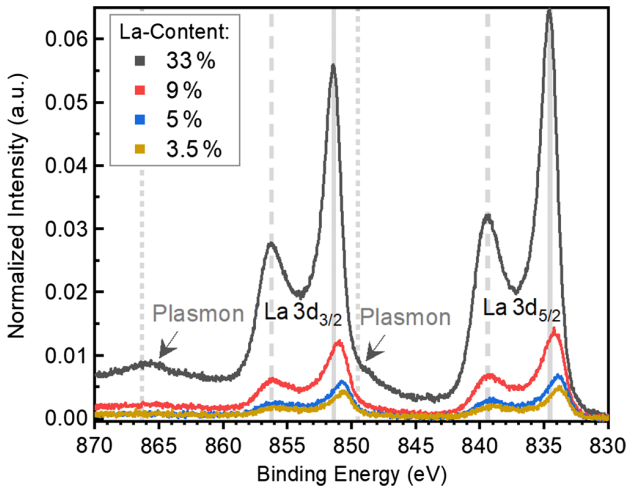

Figure 2. La 3*d* core-level spectra of four different La:HfO_2 concentrations taken at a photon energy of 6 keV. Spectra are normalized to the same Hf $4p_{3/2}$ intensity. Dotted lines denote plasmon excitations and dashed lines indicate the La 3*d* f^1 satellite peaks, shifted toward higher BE from the main 3*d* f^0 peaks.

techniques, in particular with regard to the energy resolution, nowadays, the detail of the satellite structure can be resolved.[25] The satellite peaks themselves consist of a multiplet structure originating from a coupling of spin and orbital angular moments of the f^1 state.[26,27] Although this multiplet coupling has to be taken into account for a detailed line shape analysis of the core-level spectra, the basic physical mechanisms and parameters leading to the satellite splitting, as given by Kotani et al.,[24] remain valid and may be used for a qualitative understanding.

Figure 3 shows a peak fitting analysis of the La $3d_{5/2}$ component for two different La:Hf ratios of the HfO_2 film (33% and 5%). The multiplet structure is simulated by three spectral

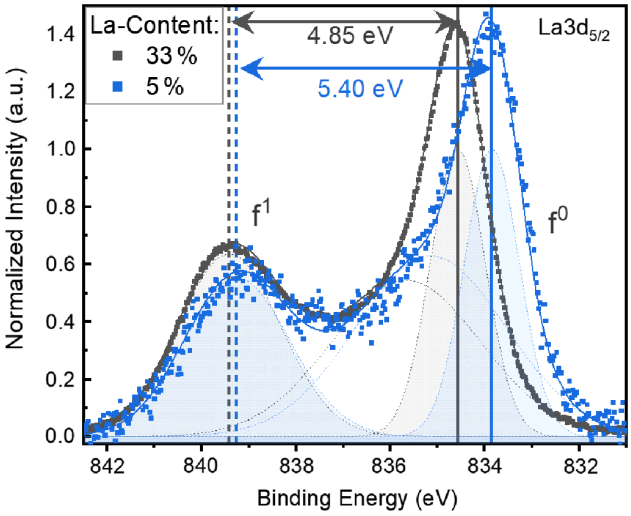

Figure 3. Peak fitting analysis of the La $3d_{5/2}$ core level for two different La concentrations. f^0 and f^1 label the two different PES final states with mainly no or one *f*-electron occupation, respectively. Binding energies and intensity ratios are listed in Table 1.

features: The components set at 834 and 839 eV are related to the f^0 and f^1 contribution, as described by Kotani et al. The broader component between them simulates additional states of the complex multiplet structure.[26,27]

As the 4*f* occupation originates from the neighboring ligand orbitals, the satellite structure of the La core levels is a direct fingerprint of its local chemical surrounding. The f^1 intensity and energy splitting from the main f^0 state reflects the overlap with and character of the ligand orbitals, respectively. The energy splitting was interpreted in terms of the character of the ligand orbital.[25,28] According to theoretical calculations by Kotani et al.,[24] the energy splitting mainly depends on the hybridization between the La 4*f* PES final states with the oxygen ligand valence orbitals. The stronger the hybridization, the larger is the energy splitting between f^0 and f^1. The intensity ratio between the f^0 and f^1 PE final state, however, depends on the 4*f* hybridization with the valence orbitals in the final as well as in the initial state. Moreover, it depends on the Coulomb interaction between the 4*f* states. The energy splitting and intensity ratios are thus not directly correlated.

Following this hybridization approach, we analyze the satellite structure of the La 3*d* spectra depending on the La content in HfO_2. We consider the energy splitting and intensity ratios of the two main peaks in the La $3d_{5/2}$ spectrum labeled as f^0 and f^1 in Figure 3. We note that this labeling—in general—is not justified because the final state has to be treated as a hybridized f^0–f^1 state, with f^0 and f^1 being its bonding and antibonding parts. In the case of La oxides, however, such labeling is valid due to the almost pure f^0 initial state.[24]

Furthermore, we determined the plasmon energy from the La 3*d* (and Hf $4p_{3/2}$) core level as depicted in Figure 2 (see also Supporting Information). Whereas satellite structures reflect local bonding characteristics to neighboring ligands, the plasmon excitation energy is a fingerprint of collective behavior of the valence band electrons. The VB electron density n and hence the plasmon energy may be modified by La doping concentration. Plasmon features are observed for all core-level spectra as a characteristic loss peak at the same loss energy E_p. In a simple approximation, E_p is given by

$$E_p = \hbar\omega_p = \hbar\sqrt{\frac{ne^2}{m\epsilon_0}} \tag{1}$$

with ω_p being the plasmon frequency, ϵ_0 the dielectric constant, e the electron charge, and m the electron mass.

La oxides mostly appear as La_2O_3 or $La_2(OH)_3$, whereby $La_2(OH)_3$ is the more stable compound in particular in the presence of water or hydroxyl. Both compounds have been investigated via XPS by Sunding et al.[25] The energy splitting Δf between the f^0 and f^1 satellites were determined as 3.9 eV for $La_2(OH)_3$ and 4.9 eV for La_2O_3, whereas a plasmon energy of 12.3 and 12.5 eV was found, respectively. We will compare our results to this data in the following.

In order to compare the different La:HfO_2-doped systems, the relevant La $3d_{5/2}$ binding energies, energy splittings, and intensity ratios obtained by a peak fit analysis and labeled in Figure 3 are listed in **Table 1**. The La $3d_{5/2}$ and La $3d_{3/2}$ components are fitted simultaneously with the same intensity ratios and splitting parameters. The spin–orbit splitting was determined as 16.86 eV

© 2022 The Authors. physica status solidi (RRL) Rapid Research Letters published by Wiley-VCH GmbH

18626270, 2022, 10, Downloaded from https://onlinelibrary.wiley.com/doi/10.1002/pssr.202100582 by Forschungszentrum Jülich GmbH Research Center, Wiley Online Library on [05/12/2022]. See the Terms and Conditions (https://onlinelibrary.wiley.com/terms-and-conditions) on Wiley Online Library for rules of use; OA articles are governed by the applicable Creative Commons License

Table 1. Peak fit parameters of the La 3*d* satellite feature dependent on the nominal La:HfO_2 concentration. The intensity ratio is determined from the integrated peak areas. The plasmon loss energy is given as a mean value obtained from the La 3*d* and Hf 4*p* excitation. In addition, the chemical shift of f^0 is listed.

La content of La:HfO_2 samples	3.5%	5%	9%	33%
La $3d_{5/2}$ f^0 binding energy	833.80 eV	833.85 eV	834.12 eV	834.57 eV
La Δf splitting	5.39 eV	5.40 eV	5.14 eV	4.85 eV
La $3d_{5/2}$ f^1/La $3d_{5/2}$ ratio	0.24	0.26	0.29	0.31
Plasmon energy $\hbar\omega_p$	15.44 eV	15.43 eV	15.20 eV	14.97 eV
Hf $4p_{3/2}$ binding energy	382.36 eV	382.32 eV	382.44 eV	382.48 eV
Chemical shift of f^0	–	0.10 eV	0.25 eV	0.66 eV

in all cases. In addition, the Hf $4p_{3/2}$ binding energies and the plasmon energies are listed.

The BE of Hf $4p_{3/2}$ increases with increasing La content. This rigid BE shift originates from a change of the Fermi-level position and is observed for all core levels related to the La:HfO_2 layer. The observed shift of the La $3d_{5/2}$ f^0 BE is larger than that of Hf $4p_{3/2}$, and indicates an additional chemical shift. This chemical shift is determined by subtracting the rigid BE shift of Hf $4p_{3/2}$ from the total f^0 BE shift, and is listed in Table 1. The f^1 component does not show a significant additional chemical shift.

We observe systematic changes of the spectral parameters dependent on the La:HfO_2 concentration. The La $3d_{5/2}$ f^1/La $3d_{5/2}$ satellite intensity ratio increases, while the Δf splitting decreases with increasing La content. For low La concentrations of 3.5% and 5%, we expect mostly similar values of the La Δf splitting because the La cations arrange as isolated defects within the HfO_2 lattice. Surprisingly, the observed change of the La Δf splitting occurs due to a shift of the f^0 component only. The small shift of the f^1 component reflects the rigid shift as also observed in the Hf $4p_{3/2}$ level. The plasmon energy ω_p decreases with increasing La concentration, indicative for a decreasing valence band electron density *n*. The ω_p for La concentrations of 3.5% and 5% of 15.44 and 15.43 eV are close to the reported values of about 15.5–16 eV for pure HfO_2.[29] However, the plasmon energy for 33% La is far above the reported value of 12.5 eV for La_2O_3. The plasmon energies were determined from the La 3*d* and Hf 4*p* core-level regions, and yield similar values (see Supporting Information).

According to calculations by Materlik et al.[12] and X-ray diffraction analysis by Schroeder et al.,[9] the La doping of HfO_2 was considered as pure hole doping. In this model, each La cation creates a hole in the valence band, without any compensation by OV charges. Taking into account the broad range of doping concentrations investigated in this study, it should result in a considerable change of the Fermi level. However, the observed rigid core-level shift, which is equivalent to such a Fermi-level shift, is negligible. Even the reduction of the electron density in the valence band deduced from the plasmon energy seems to be far too small for a La concentration up to 33%. Thus, the hole charge in the valence band created by La doping seems to be compensated, and OV should be taken into account.[12,20]

A central question is whether such an interaction occurs from intrinsic OV or whether additional ones must have been created. Intrinsic OVs in HfO_2 are typically in a 2+ state and emerge in the form of Hf^{3+} signatures. Thus, an exchange of Hf^{3+} by La^{3+} would barely change the electronic structure. However, any Hf^{3+} signatures observed in HAXPES spectra should be reduced. In contrast, Hamouda et al. observed an increase of the Hf^{3+} signature in the Hf 3*d* spectra of HZO for La concentrations between 1% and 3%.[30] However, these values are far below the La concentrations considered in this study, and HZO itself might reveal different electronic properties at the Fermi level.[31]

Our observed energy splitting and intensity ratio of the La 3*d* satellite structure can be compared to calculations by Kotani et al. and previously published experimental La 3*d* spectra. With regard to La_2O_3 and $La_2(OH)_3$, our observed spectral parameter for the La $3d_{5/2}$ peak significantly differs from these values, indicating a different local chemical surrounding. Excluding the 33% sample, all Δf energy splittings are significantly larger than the splittings reported in the literature for La_2O_3 and $La_2(OH)_3$.[25] According to Kotani, the decrease of the Δf splitting with increasing La concentration indicates a decreasing hybridization between La 4*f* states and the oxygen valence band of HfO_2. This is in accordance with the observed small increase of the satellite intensity ratio. The observed splitting for the 33% sample, however, is comparable to the La_2O_3 literature values, but our observed satellite intensity is significantly lower. The reported La 3*d* spectra of the pyrochlore $La_2Hf_2O_7$ phase[15] compares well in terms of splitting as well as intensity ratio. Furthermore, our observed plasmon energy is significantly larger than determined by Sunding et al. for La_2O_3 and $La_2(OH)_3$, which reveals a higher electron density in the valence band. As already mentioned above, the $La_2Hf_2O_7$ phase may be electronically considered as a 50% doping, which is completely compensated by a vacancy.

Finally, we consider the La 4s spectrum. The *s*-spectra of transition metals are usually treated as the simplest example of the interaction of a PE core hole with an open shell due to its

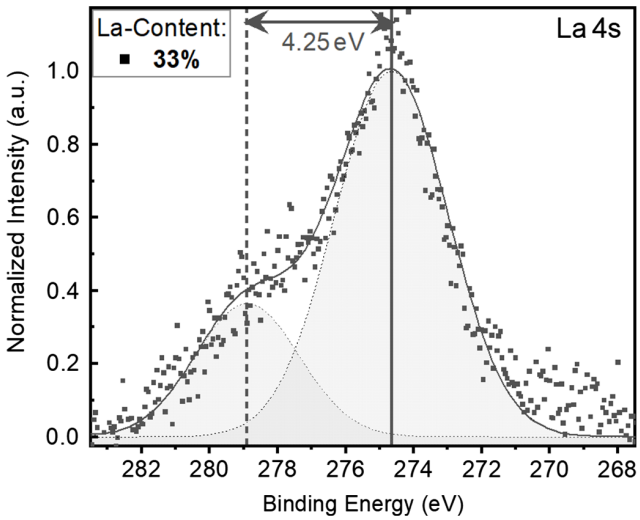

Figure 4. Peak fit analysis of the background-corrected La 4*s* core level. The area ratio of both peaks is 1:3. The two different PE final states belong to none or one *f*-electron occupation, respectively.

© 2022 The Authors. physica status solidi (RRL) Rapid Research Letters published by Wiley-VCH GmbH

18626270, 2022, 10, Downloaded from https://onlinelibrary.wiley.com/doi/10.1002/pssr.202100582 by Forschungszentrum Jülich GmbH Research Center, Wiley Online Library on [05/12/2022]. See the Terms and Conditions (https://onlinelibrary.wiley.com/terms-and-conditions) on Wiley Online Library for rules of use; OA articles are governed by the applicable Creative Commons License

vanishing orbital momentum. **Figure 4** shows the background-corrected La 4*s* PES spectrum from the sample with 33% La. In analogy to the La 3*d* spectra, the low BE peak might be related to the f^0 component, whereas the peak on the high BE side might represent the f^1 component. However, it is worth mentioning that the 4*s*-level spectrum can also be understood without considering a $4f^0$ component, just as a final state coupling of the 4*s* core hole with the $4f^1$ state, as considered for 3*d* and other 4*f* elements. The multiplet splitting in the *s*-level PE spectra in this model consists of two components related to the two possibilities of the core hole spin s_c to couple to the *f*-electron spin s_f, i.e., $S = s_f + s_c$ or $S = s_f - s_c$. The intensity ratio of the two peaks should be given by the multiplicity of the two states. Assuming a single occupied *f*-level, a ratio of 3/1 is expected, which nearly perfectly fits the observed ratio. The observed energy splitting related to the 4*s*–4*f* exchange coupling amounts to 4.25 eV.

3. Conclusion

From a HAXPES analysis of La 3*d* and Hf 4*f* core-level spectra, we concluded on the electronic incorporation of La dopants into the HfO_2 lattice, covering La doping concentration from 3.5% to 33%. We analyzed the La 3*d* satellite structure in terms of hybridization between La 4*f* states with the O 2*p* valence states, which gives insights into the local chemical surrounding of the La lattice sites. Moreover, the rigid core-level BE shift and the plasmon excitation energies allow to conclude on the collective electronic properties of La doping.

We applied the widely accepted model by Kotanti et al.,[24,26] which relates core-level multiplet structures of La compounds to hybridized 4*f* and valence orbitals as a PE final state effect. Core-level doublet structures are interpreted as bonding and antibonding states of this hybridization. Accordingly, we explain the observed decreasing satellite splitting with increasing La content to a decreasing hybridization between La 4*f* and O 2*p* valence band orbitals. In turn, the La–O bond length should increase because the orbital overlap decreases. From the difference between our observed intensity ratios between f^0 and f^1 and the already published spectra of La_2O_3 and $La_2(OH)_3$,[25] we conclude on a different chemical surrounding of the La ions, although the f^0–f^1 splitting in case of 33% La content is comparable to La_2O_3. A charge transfer from interface charges cannot be excluded but, if present, it is expected to be the same for all La doping concentrations. The observed change in the band alignment is small compared to the satellite splitting and thus a charge transfer has not been taken into account.

In accordance with theoretical calculations on the stabilization of the ferroelectric phase[10–12] we suggest the structural incorporation of La into the HfO_2 lattice by a substitution of Hf by La at the Hf site, at least up to a La concentration of about 10%. For higher La concentrations, the formation of a pyrochlore $La_2Hf_2O_7$ phase as reported by Smirnova et al.[15] is in accordance with our HAXPES results. However, we cannot confirm the existence of a La_2O_3 phase in HfO_2. For the collective effects like Fermi-level shift and plasmon excitation, we observe only small changes that do not reflect the broad range of La doping concentrations as investigated. Here, we assume that the so-called doping limit is reached for large La concentrations. In this case, the valence band holes, which are created by the La^{3+} doping, are compensated by OV electrons. Whether these vacancies are intrinsic or additionally created ones remains an open question.

Our analysis of the local chemistry and collective electronic properties by HAXPES confirms the theoretical predictions of La doping on the stabilization of the ferroelectric phase of HfO_2. In addition, the spectroscopically observed electronic compensation of vacancy charges shall decrease the detrimental influence of OVs on the ferroelectic properties. In general, this beneficial combination of both structural and electronic compensation of OVs by La doping strongly suggests a significant improvement of La:HfO_2-based ferroelectric devices in terms of durability.

4. Experimental Section

Lanthanum-doped HfO_2 thin films of $d = 12 - 15$ nm were grown by ALD using tetrakis(ethylmethylamino)hafnium ($Hf[N(CH_3)(C_2H_5)]_4$) and tris(isopropyl-cyclopentadienyl)lanthanum (La-$(iPrCp)_3$) as metal precursors. In both cases, water was used as reactant. Different doping concentrations were achieved by adjusting the layer stacking ratio between Hf and La. We investigated samples with a stacking ratio of one La layer versus 2, 10, 18, or 28 HfO_2 layers. These ratios are equivalent to nominal La concentrations of about 33%, 9%, 5%, and 3.5%.

The nominally expected La concentrations were compared with the observed intensity ratios of the La 3*d* and Hf 4*s* core-level spectral weights as observed by HAXPES. Both ratios should differ only by a constant factor, which reflects the different photoelectric cross sections of the La 3*d* and Hf 4*s* core levels. Only small differences without any systematic deviations were observed, thus confirming the nominal La concentration.

TiN bottom and top electrodes were grown by physical vapor deposition (PVD) in a separate deposition chamber.

HAXPES was performed at the P22 beamline of PETRA III (DESY, Hamburg)[32] to investigate element-selective chemical properties. Spectra of Hf 4*f*, La 3*d* and 4*s*, Ti 2*p*, and O 2*p* core levels were recorded using linearly polarized light at a photon energy of 6 keV. HAXPES thereby provides the large information depth of about 20 nm to probe the HfO_2 layer together with the top electrode of the capacitor stack. A SPECS PHOIBOS electron analyzer was used at an emission angle of 10° and a pass energy of 30 eV, resulting in an overall energy resolution of about 300 meV.

Acknowledgements

This project has received funding from the European Union's Horizon 2020 research and innovation program under grant agreement no. 780302. The authors acknowledge DESY (Hamburg, Germany), a member of the Helmholtz Association HGF, for the provision of experimental facilities. Funding for the HAXPES instrument at beamline P22 by the Federal Ministry of Education and Research (BMBF) under contracts 05KS7UM1 and 05K10UMA with Universität Mainz; 05KS7WW3, 05K10WW1, and 05K13WW1 with Universität Würzburg is gratefully acknowledged.

Open access funding enabled and organized by Projekt DEAL.

Conflict of Interest

The authors declare no conflict of interest.

Data Availability Statement

The data that support the findings of this study are available from the corresponding author upon reasonable request.

© 2022 The Authors. physica status solidi (RRL) Rapid Research Letters published by Wiley-VCH GmbH

18626270, 2022, 10, Downloaded from https://onlinelibrary.wiley.com/doi/10.1002/pssr.202100582 by Forschungszentrum Jülich GmbH Research Center, Wiley Online Library on [05/12/2022]. See the Terms and Conditions (https://onlinelibrary.wiley.com/terms-and-conditions) on Wiley Online Library for rules of use; OA articles are governed by the applicable Creative Commons License

Keywords

3*d* multiplet, doping limit, hard X-ray photoelectron spectroscopy, La:HfO_2, vacancies

Received: November 15, 2021
Revised: February 1, 2022
Published online: February 20, 2022

[1] H. Kohlstedt, Y. Mustafa, A. Gerber, A. Petraru, M. Fitsilis, R. Meyer, U. Böttger, R. Waser, in *14th Biennial Conf. on Insulating Films on Semiconductors*, Elsevier, Amsterdam, Leuven, Belgium Vol. *80*, **2005**, p. 296.
[2] F. P. G. Fengler, M. Pešić, S. Starschich, T. Schneller, U. Böttger, T. Schenk, M. H. Park, T. Mikolajick, U. Schroeder, in *2016 46th European Solid-State Device Research Conf. (ESSDERC)*, IEEE, Lausanne, Switzerland **2016**, pp. 369–372.
[3] M. H. Park, Y. H. Lee, T. Mikolajick, U. Schroeder, C. S. Hwang, *MRS Commun.* **2018**, *8*, 795.
[4] T. S. Böscke, J. Müller, D. Bräuhaus, U. Schröder, U. Böttger, *Appl. Phys. Lett.* **2011**, *99*, 102903.
[5] T. Mittmann, M. Materano, P. D. Lomenzo, M. H. Park, I. Stolichnov, M. Cavalieri, C. Zhou, C.-C. Chung, J. L. Jones, T. Szyjka, M. Müller, A. Kersch, T. Mikolajick, U. Schroeder, *Adv. Mater. Interfaces* **2019**, *6*, 1900042.
[6] M. Materano, P. D. Lomenzo, A. Kersch, M. H. Park, T. Mikolajick, U. Schroeder, *Inorg. Chem. Front.* **2021**, *8*, 2650.
[7] M. H. Park, D. H. Lee, K. Yang, J.-Y. Park, G. T. Yu, H. W. Park, M. Materano, T. Mittmann, P. D. Lomenzo, T. Mikolajick, U. Schroeder, C. S. Hwang, *J. Mater. Chem. C* **2020**, *8*, 10526.
[8] L. Baumgarten, T. Szyjka, T. Mittmann, M. Materano, Y. Matveyev, C. Schlueter, T. Mikolajick, U. Schroeder, M. Müller, *Appl. Phys. Lett.* **2021**, *118*, 3.
[9] U. Schroeder, C. Richter, M. H. Park, T. Schenk, M. Pešić, M. Hoffmann, F. P. G. Fengler, D. Pohl, B. Rellinghaus, C. Zhou, C.-C. Chung, J. L. Jones, T. Mikolajick, *Inorg. Chem.* **2018**, *57*, 2752.
[10] R. Batra, T. D. Huan, J. L. Jones, G. Rossetti, R. Ramprasad, *J. Phys. Chem. C* **2017**, *121*, 4139.
[11] R. Batra, T. D. Huan, G. A. Rossetti, R. Ramprasad, *Chem. Mater.* **2017**, *29*, 9102.
[12] R. Materlik, C. Künneth, M. Falkowski, T. Mikolajick, A. Kersch, *J. Appl. Phys.* **2018**, *123*, 164101.
[13] M. H. Park, Y. H. Lee, T. Mikolajick, U. Schroeder, C. S. Hwang, *Adv. Electron. Mater.* **2019**, *5*, 1800522.
[14] T. V. Perevalov, A. K. Gutakovskii, V. N. Kruchinin, V. A. Gritsenko, I. P. Prosvirin, *Mater. Res. Express* **2018**, *6*, 036403.
[15] T. Smirnova, L. Yakovkina, V. Borisov, *J. Rare Earths* **2015**, *33*, 857.
[16] M. Müller, S. Nemšák, L. Plucinski, C. M. Schneider, *J. Electron Spectrosc. Rel. Phenom.* **2016**, *208*, 24.
[17] M. Müller, P. Lömker, P. Rosenberger, M. H. Hamed, R. A. Mueller, D. N. Heinen, T. Thomas Szyjka, L. Baumgarten, *J. Vacuum Sci. Technol. A* **2021**.
[18] T. Szyjka, L. Baumgarten, T. Mittmann, Y. Matveyev, C. Schlueter, T. Mikolajick, U. Schroeder, M. Müller, *ACS Appl. Electron. Mater.* **2020**, *2*, 3152.
[19] T. Szyjka, L. Baumgarten, T. Mittmann, Y. Matveyev, C. Schlueter, T. Mikolajick, U. Schroeder, M. Müller, *Phys. Status Solidi (RRL)* **2021**, *15*, 2100027.
[20] D. Liu, J. Robertson, *Appl. Phys. Lett.* **2009**, *94*, 042904.
[21] H. Li, Y. Guo, J. Robertson, *Appl. Phys. Lett.* **2014**, *104*, 192904.
[22] O. Gunnarsson, K. Schönhammer, *Phys. Rev. B* **1983**, *28*, 4315.
[23] J. C. Fuggle, F. U. Hillebrecht, Z. Zołnierek, R. Lässer, C. Freiburg, O. Gunnarsson, K. Schönhammer, *Phys. Rev. B* **1983**, *27*, 7330.
[24] A. Kotani, M. Okada, T. Jo, A. Bianconi, A. Marcelli, J. C. Parlebas, *J. Phys. Soc. Jpn.* **1987**, *56*, 798.
[25] M. Sunding, K. Hadidi, S. Diplas, O. Løvvik, T. Norby, A. Gunnæs, *J. Electron Spectrosc. Rel. Phenomena* **2011**, *184*, 399.
[26] A. Kotani, H. Ogasawara, *J. Electron Spectrosc. Rel. Phenomena* **1992**, *60*, 257.
[27] D. F. Mullica, C. K. C. Lok, H. O. Perkins, V. Young, *Phys. Rev. B* **1985**, *31*, 4039.
[28] T. Perevalov, V. Gritsenko, D. Islamov, I. Prosvirin, *JETP Lett.* **2018**, *107* 55.
[29] H. Jin, S. K. Oh, H. J. Kang, S. Tougaard, *J. Appl. Phys.* **2006**, *100*, 083713.
[30] W. Hamouda, C. Lubin, S. Ueda, Y. Yamashita, O. Renault, F. Mehmood, T. Mikolajick, U. Schroeder, R. Negrea, N. Barrett, *Appl. Phys. Lett.* **2020**, *116*, 252903.
[31] L. Zhao, J. Liu, Y. Zhao, *Appl. Phys. Lett.* **2021**, *119*, 172903.
[32] C. Schlueter, A. Gloskovskii, K. Ederer, I. Schostak, S. Piec, I. Sarkar, Y. Matveyev, P. Lömker, M. Sing, R. Claessen, C. Wiemann, C. M. Schneider, K. Medjanik, G. Schönhense, P. Amann, A. Nilsson, W. Drube, S. Gwo, D.-J. Huang, D.-H. Wei, *AIP Conf. Proc.* **2019**, *2054*, 040010.

© 2022 The Authors. physica status solidi (RRL) Rapid Research Letters published by Wiley-VCH GmbH

18626270, 2022, 10, Downloaded from https://onlinelibrary.wiley.com/doi/10.1002/pssr.202100582 by Forschungszentrum Jülich GmbH Research Center, Wiley Online Library on [05/12/2022]. See the Terms and Conditions (https://onlinelibrary.wiley.com/terms-and-conditions) on Wiley Online Library for rules of use; OA articles are governed by the applicable Creative Commons License